

ADVERSARIAL EXAMPLES AND WHERE TO FIND THEM

PREPRINT, COMPILED MARCH 31, 2022

NIKLAS RISSE*

CHRISTINA GÖPFERT*

JAN PHILIP GÖPFERT*

Bielefeld University, Germany

ABSTRACT

Adversarial robustness of trained models has attracted considerable attention over recent years, within and beyond the scientific community. This is not only because of a straight-forward desire to deploy reliable systems, but also because of how adversarial attacks challenge our beliefs about deep neural networks. Demanding more robust models seems to be the obvious solution – however, this requires a rigorous understanding of how one should judge adversarial robustness as a property of a given model. In this work, we analyze where adversarial examples occur, in which ways they are peculiar, and how they are processed by robust models. We use robustness curves to show that ℓ_∞ threat models are surprisingly effective in improving robustness for other ℓ_p norms; we introduce perturbation cost trajectories to provide a broad perspective on how robust and non-robust networks perceive adversarial perturbations as opposed to random perturbations; and we explicitly examine the scale of certain common data sets, showing that robustness thresholds must be adapted to the data set they pertain to. This allows us to provide concrete recommendations for anyone looking to train a robust model or to estimate how much robustness they should require for their operation. The code for all our experiments is available at www.github.com/niklasrisse/adversarial-examples-and-where-to-find-them.

1 INTRODUCTION

Adversarial robustness is a property that describes a model’s ability to behave correctly under small input perturbations that are crafted with the intent to mislead the model. In recent years, it has been pointed out that deep neural networks, despite their astonishing success in a wide range of prediction tasks, frequently lack this property [17, 8]. The study of adversarial robustness – with its definitions, their implications, attacks, and defenses – has subsequently attracted considerable research interest. This is due both to the practical importance of trustworthy models and the intellectual interest in the differences between decisions of machine learning models and our human perception.

From a theoretical perspective, this scientific enthusiasm has led to an analysis of different definitions of adversarial robustness, their implications in terms of sample complexity and computational hardness, and the possibility or impossibility of achieving adversarial robustness under certain distributional assumptions [7, 11]. These results on hardness pose an intellectual challenge: for many domains, a robust and efficient classifier does exist in the human brain (indeed, adversarial examples are often motivated by the differences between human and model classification). If we are not yet able to replicate this artificially, is it due to our definitions, our models, our data representation, or our optimization procedures?

From a practical perspective, we have seen the development of a wide array of defenses against adversarial attacks, most of which have quickly prompted the development of new attack methods capable of circumventing them [2, 4, 15, 19, 3]. A helpful overview of methodological foundations for defense mechanisms (and thereby indirectly of attack mechanisms) is given by [3]. Central to the development of an adversarial defense is the specification of a *threat model* that defines the types of perturbations which, when applied to real data points, should

not change the classification behavior of the model. The challenge then lies in finding a tractable optimization procedure that satisfies the threat model, and in providing credible empirical or – ideally – theoretical evidence to show that the resulting model is indeed robust to all perturbations in the threat model. The most commonly used threat models are ℓ_p ball constrained perturbations, i. e. perturbations with ℓ_p norm smaller than a specified threshold. The most commonly used norms in this context are ℓ_∞ , ℓ_2 and ℓ_1 . Under this type of threat model, by definition, the study of adversarial robustness is closely tied to the distance of examples to decision boundaries. Constructing models where adversarial perturbations are rare, then involves directly or indirectly maximizing margins around decision boundaries¹.

One popular defense mechanism for indirectly maximizing margins is Adversarial Training with Projected Gradient Descent (AT), which Madry et al. [15] argue provides a natural security guarantee against first-order adversaries motivated by robust optimization. Wong and Kolter [20] introduce a method (KW) with provable robustness against any norm-bounded perturbation on the training data by adapting the training process to minimize an upper bound on the robust loss of the network. Croce et al. [5] and Croce and Hein [6] achieve improved robustness to ℓ_p norm bounded perturbations by adding a regularization term that penalizes closeness to decision boundaries and linear regions of the model (MMR + AT and MMR-UNIV).

For this work, we explicitly decided not to focus on developing a new adversarial attack or defense. Instead, we explore and present adversarial robustness from a broader perspective, in order to increase the community’s understanding of how defense methods interact with choice of threat model, properties of the data set, and the way adversarials are processed. We start by

*equal contribution

¹It should – therefore – not surprise us when algorithms, such as the Support Vector Machine, that by construction maximize margins, also lead to adversarially robust models regarding the type of margin they optimize.

describing robustness curves [9] in Section 2 as a tool to evaluate the robustness of specific models and data sets and then study how robustness depends on distance function, data distribution and training method. The main part of the paper is structured as follows:

1. In Section 3, we compare robustness curves for different models and different choices of distance functions. Our goal is to understand how the choice of model and training method impacts robustness, and to what extent robustness transfers between distance functions. For linear classifiers we show theoretically, that the shape of the robustness curve – representing the global robustness behaviour – is the same for all norms, and closeness of the norms can be controlled via sparsity of the weight vector. For non-linear models we empirically find that robustness transfers to ℓ_p norms not considered in the threat model, and the ℓ_∞ threat models frequently provide better ℓ_2 robustness than ℓ_2 threat models.
2. In Section 4, we analyze how adversarial perturbations are perceived by robust and non-robust networks, specifically compared to random perturbations. To gain insight, we introduce perturbation cost trajectories, which offer a broader perspective on how a network perceives an input, and we find that adversarial perturbations propagate through deep networks in peculiar ways.
3. Finally, in Section 5, we analyze how scale depends on the underlying data space, choice of distance function, and distribution. The main results are that the robustness curve for one norm-induced distance places bounds on the robustness curves for all other norm-induced distances and that the separation between curves can be extremely large, depending on the model and underlying data distribution. Based on these findings we suggest that the maximum perturbation size of threat models should be selected carefully in order to be meaningful, depending on characteristics of the data set.

2 ROBUSTNESS CURVES

Let us consider what we would actually hope to see when performing an adversarial attack, instead of the small performance-breaking perturbations one encounters. We would hope to see either a meaningful – but small – alteration of the original input, such as an airplane growing eyes, a beak, and plumage, to be classified as a bird; or a complete dismantling of meaningful features resulting in unrecognizable noise, where we can readily accept pseudo-random class predictions. Semantics are crucial in both scenarios, which leads us to the conviction that our human perception and classification are integral to the nature of adversarial examples. Still, we must work with a more rigorous definition and therefore abstract further, which we do in the following.

An adversarial perturbation for a classifier f and input-output pair (x, y) is a small perturbation δ with $f(x + \delta) \neq y$. The resulting input $x + \delta$ is called an adversarial example. The set of input-output pairs vulnerable to adversarial perturbations is

the set of data points which the classifier can be induced to misclassify using small perturbations – that is the set of points that are either already misclassified, or that lie in some small distance from the decision boundary. But what does *small* mean? How should *distance* be measured? And what distinguishes adversarial examples from other data points? These are the questions we aim to answer in the following sections.

One tool for our study of these questions are *robustness curves* [9], which we shortly explain in this section. A robustness curve is the cumulative distribution function of the distance of points from the decision boundaries of a classifier:

Definition 1. Given an input space X and label space \mathcal{Y} , distance function d on $X \times X$, and classifier $f : X \rightarrow \mathcal{Y}$. Let $|\mathcal{X}| = \max_{x, x' \in X} d(x, x')$ and let P denote the data distribution that generates the samples. Then the d -robustness curve for f is the graph of the function

$$R_d^f : [0, |\mathcal{X}|] \rightarrow [0, 1]$$

$$\varepsilon \mapsto P(\{(x, y) \text{ s.t. } \exists x' : d(x, x') \leq \varepsilon \wedge f(x') \neq y\})$$

A model’s robustness curve shows how data points are distributed in relation to the decision boundaries of the model. The advantage of this distributional perspective is that it allows a step back from robustness regarding a specific quantification of what it means to be close to the decision boundary, and instead allows us to compare global robustness properties and their dependence on a given classifier, distribution and distance function. One of the main questions driving this work is how robustness – and robust training – are affected by the choice of distance function.

In principle, there exist a wealth of possible distance functions, and the choice of one particular distance function should depend on the downstream application domain of the model. For this work, we will assume that the distance function d is induced by some norm n on X , i. e. $d(x, x') = n(x - x')$. As Göpfert et al. [10] show, this is not sufficient to encode dissimilarities of images as perceived by a human, or guarantee that perturbations are imperceptible to the human eye. However, the majority of current work on robustness uses distances induced by ℓ_p norms [19]. They are easy to define and well studied, and it is reasonable to assert that perturbations that are small in some ℓ_p norm typically should not change the classification of real-world images. In the following, we always assume that the distance we consider is induced by some norm, usually an ℓ_p norm, on a finite-dimensional vector space. In our experiments we consider the ℓ_1 , ℓ_2 and ℓ_∞ norms, as these are frequently used prototypical examples.

3 ROBUSTNESS CURVES AND THEIR DEPENDENCE ON DISTANCE FUNCTIONS

Due to strong concerns about trust in and security of machine learning models that are susceptible to adversarial perturbations, the last years have seen significant effort in developing training methods that produce more robust models. These training methods typically require the choice of a distance function d and perturbation threshold ε . The pair (d, ε) is sometimes called a threat model. The training method will attempt (and possibly guarantee) to make the model robust against attacks in distance

d up to size ε . In other words, the objective of the training method is to minimize $R_d^f(\varepsilon)$. In the following, we analyze to what extent the minimization of $R_d^f(\varepsilon)$ impacts $R_{d'}^f(\varepsilon')$ for other choices d' and ε' .

For the special case of linear classifiers, we find that the global robustness behavior of a model w. r. t. a data distribution for *all* ℓ_p norms is fully specified by the model parameters and the robustness curve for a *single* ℓ_p norm. Thus, we fully understand the behavior of $R_{d'}^f(\varepsilon')$ for any ℓ_p norm induced distance d' and any ε' based on knowing $R_d^f(\cdot)$ for one ℓ_p norm induced distance d . This is an extension of a weaker theorem from [9].

Theorem 1. *If f is a linear classifier on \mathbb{R}^d parameterized by (\vec{w}, b) , i. e. $f(x) = \text{sgn}(\vec{w}^T x + b)$, then the shape of the robustness curve for f regarding an ℓ_p norm-induced distance does not depend on the choice of p . There exists a constant $c > 0$ such that*

$$R_{\|\cdot\|_{p_1}}^f(\varepsilon) = R_{\|\cdot\|_{p_2}}^f(c \cdot \varepsilon) \quad \forall \varepsilon. \quad (1)$$

The distortion factor c is given by $\frac{\|\vec{w}\|_{q_1}}{\|\vec{w}\|_{q_2}}$, where $q_i = \frac{p_i}{p_i-1}$.

We provide a proof in Appendix A. Clearly, the distortion factor c can be as large as m , where m is the dimensionality of the input space. See Appendix B.2 for an example where this occurs. One way to minimize this distortion factor is to encourage sparse weight vectors. However, as illustrated by Appendix B.2, this may backfire by worsening robustness for norms the model would otherwise be robust to, instead of improving robustness for norms it would otherwise not be robust to.

For more complex decision boundaries, dependence on p can be more than a question of scale. The *shape* of the robustness curve may depend on p , i. e. the distribution of the distances between points and decision boundary may be different for different choices of p . See Figure 1 for an example. In the following, we empirically evaluate robustness curves for different models to investigate how robustification efforts transfer across norms. For complex models, exactly calculating the distance of a point to the closest decision boundary, and thus estimating the robustness curve, is computationally very intensive, if not intractable. Instead, we bound the true robustness curve from below using adversarial attacks. To verify that this approach is justified, we compare a robustness curve estimated using adversarial attacks to one based on exact calculation of distances to the decision boundary on a simple robust model. We observe that the shape and scale of the curves are very similar, especially for small perturbation sizes, which are most relevant in assessing the robustness of the model. See Appendix D.1 for detailed results. We compare ℓ_∞ and ℓ_2 robustness curves for different robustified models from the literature. The network architecture we use in our analysis is a convolutional network with two convolutional layers, two fully connected layers and ReLU activation functions. We compare the following training methods:

1. Standard training (ST), i. e. training without specific robustness considerations.
2. Adversarial training (AT), see Madry et al. [15].
3. Training with robust loss (KW), see Wong and Kolter [20].

4. Maximum margin regularization for a single ℓ_p norm together with adversarial training (MMR + AT), see Croce et al. [5]
5. Maximum margin regularization simultaneously for ℓ_∞ and ℓ_1 margins (MMR-UNIV), see Croce and Hein [6].

Together with each training method, we state the threat model the model is optimized to guarantee (e. g. Threat Model: $\ell_\infty(\varepsilon = 0.1)$ for robustness guarantees in ℓ_∞ norm for $\ell_\infty = 0.1$), if available. Unless explicitly stated otherwise, the trained models are those made publicly available² by Croce et al. [5] and Croce and Hein [6]. We use six datasets: MNIST, Fashion-MNIST (FMNIST), German Traffic Signs (GTS) [12], CIFAR-10, Tiny-Imagenet-200 (TINY-IMG) [14], and Human Activity Recognition (HAR) [1]. For specifics on model training, refer to Appendix C. Models are generally trained on the full training set for the corresponding data set, and robustness curves evaluated on the full test set, unless stated otherwise. See Appendix D.2 for examples of adversarial perturbations optimized for different norms and different models, which provides intuition on how norm constraints and adversarial defenses affect adversarial perturbations.

First, we compute ℓ_2 and ℓ_∞ robustness curves on MNIST for the five different training methods mentioned above, each for ℓ_2 and ℓ_∞ threat models, except for MMR-UNIV which simultaneously defends against attacks in all ℓ_p norms. The results can be seen in Figure 2. We find that for AT and MMR + AT, the ℓ_∞ threat model leads to better robustness than the ℓ_2 threat model *both* for ℓ_∞ and ℓ_2 robustness curves. In fact, MMR + AT with the ℓ_∞ threat model even leads to better ℓ_∞ and ℓ_2 robustness curves than MMR-UNIV, which is specifically designed to improve robustness for all ℓ_p norms. For KW, interestingly the ℓ_∞ threat model leads to better ℓ_∞ robustness than the ℓ_2 threat model only for perturbation sizes up to around 0.15, and the ℓ_2 threat model only leads to better ℓ_2 robustness than the ℓ_∞ threat model up to perturbation size around 1.2, after which the two curves intersect. For all three training methods under the ℓ_∞ threat model, we observe a noticeable change in slope of the ℓ_∞ robustness curve between perturbation sizes 0.1 and 0.2 (perturbation size in the threat model chosen to be 0.1 in each case). MMR + AT is significant in that the change in slope occurs later than in the other models, even though the target perturbation size is identically 0.1. Each method leads to significantly improved robustness curves as compared to ST, even beyond the perturbation sizes specified by the threat model.

Because perturbations sizes in ℓ_∞ and ℓ_2 norm tend to be very different, it is difficult to compare robustness curves for the two norms in a single plot. In Figure 3, we introduce two methods of rescaling to better compare the shapes of the curves. With method 1, we rescale the ℓ_∞ robustness curve by the mean ratio $\frac{R_{\|\cdot\|_2}(\varepsilon)}{R_{\|\cdot\|_\infty}(\varepsilon)}$ between the curves. This method allows us to see even more clearly how the ℓ_∞ robustness curve for MMR + AT with ℓ_∞ threat model changes slope around the target perturbation size, which does not occur in the ℓ_2 robustness curve for any of the training methods. With method 2, we rescale the ℓ_∞ robustness curve by the mean ratio $\frac{\|x\|_2}{\|x\|_\infty}$ for all points x in the data set. The benefit of this rescaling method is that it does not require

²www.github.com/fra31/mmr-universal, www.github.com/max-andr/provable-robustness-max-linear-regions

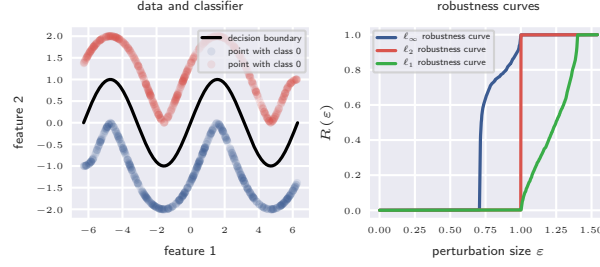


Figure 1: A model with a non-linear decision boundary and three differently shaped robustness curves.

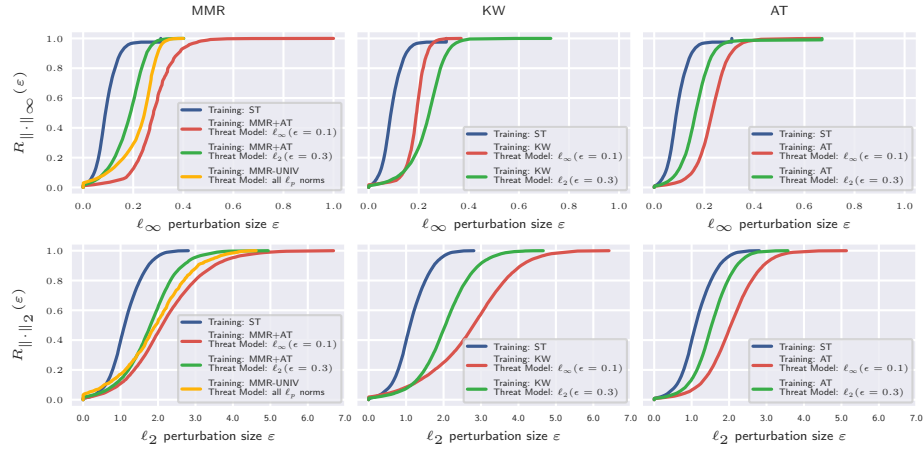
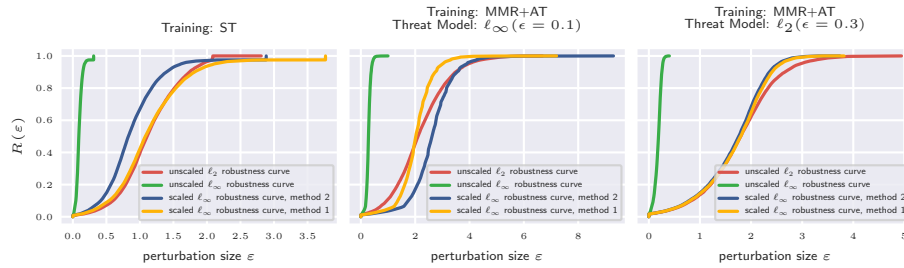
Figure 2: Robustness curves resulting from different training methods (MMR + AT, MMR-UNIV (first column), KW (second column), and AT (third column), always with ST for comparison) and different threat models (indicated by color), measured in the ℓ_∞ norm (first row) and the ℓ_2 norm (second row).

Figure 3: Scaled and unscaled robustness curves for different training methods. Scaling methods are indicated by color. Training methods are indicated by plot titles.

computation of both curves, but, at least empirically, can still provide an estimate of the ℓ_2 robustness curve or vice versa. It is interesting to see that method 2 overestimates the ℓ_2 robustness curve for ST, underestimates it for MMR + AT with the ℓ_∞ threat model, and almost perfectly estimates it for MMR + AT with the ℓ_2 threat model. This reinforces that compared to standard training, MMR + AT with both the ℓ_∞ and ℓ_2 threat models improve ℓ_∞ robustness more strongly than ℓ_2 robustness.

Figure 4 shows ℓ_∞ robustness curves for MMR + AT with ℓ_∞ threat model as provided by Croce et al. [5]. The models trained on MNIST and FMNIST both show the characteristic change in slope. Further, the robustness curves for CIFAR-10 and GTS show that the models for these two data sets, which were trained with much smaller target perturbation sizes, are very non-robust compared to the former two models and do not have a visually detectable change in slope. We will revisit the question of which target perturbation level to choose in dependence on the data set in Section 5.

4 HOW ADVERSARIAL PERTURBATIONS ARE PROCESSED

In the previous section, our focus was on how robust training methods impact the robustness curve of the resulting model. Now, we investigate how they impact the way the neural network “perceives” adversarial perturbations. Instead of only looking at the perturbed input and the resulting (mis-)classification, we follow the effects of a perturbation along every step along its way through the network – i. e. at each layer. As a tool for this, we introduce *perturbation cost trajectories*.

Definition 2. Let $f : \mathbb{R}^m \rightarrow \mathbb{R}^l$ be the function calculated by a neural network, where m is the input dimensionality, l is the cardinality of the label space, and the output of f are the softmax probabilities for each class. Let k be the number of layers in the network. For $x \in \mathbb{R}^m$ and $i \in \{0, \dots, k\}$ let $f_i(x)$ denote the output of the first i layers of the network, applied to x . In particular, $f_0(x) = x$ and $f_k(x) = f(x)$. Let x be an input to the network, let $\Delta \in \mathbb{R}^m$ be a perturbation and let $\|\cdot\|$ denote a norm. Then the perturbation cost of Δ for x at layer $i \in \{1, \dots, k-1\}$ is defined as

$$C_x^i(\Delta) := \frac{\|f_i(x + \Delta) - f_i(x)\|}{\|f_i(x)\|}. \quad (2)$$

The perturbation cost of Δ at layer k is $C_x^k(\Delta) = \mathbb{1}_{f(x+\Delta) \neq f(x)}$. The perturbation cost trajectory of Δ at x is the sequence $(C_x^i(\Delta))_{i=1}^k$.

Adversarial versus random perturbations

In the following, we present and discuss several perturbation cost trajectories for a simple architecture trained with either ST or MMR + AT³. We perturb 1000 data points from the MNIST test set and feed them through the network – then, for comparison, we sample random perturbations of the exact same size and trace those through the network⁴. For each trained model, this yields two pairs of curves – one for the ℓ_∞ norm and one for

the ℓ_2 norm. Perturbation cost trajectories are computed w. r. t. the norm that the perturbation is optimized for. This allows a number of observations (cf. Figure 5):

1. For all three models, data points perturbed with random noise are almost never misclassified, compared to (by construction) all data points with adversarial perturbations.
2. Only perturbation costs of ℓ_2 scaled perturbations decrease monotonously with each additional layer.
3. In the non-robust network, perturbation costs for adversarial perturbations are amplified by each layer.
4. Perturbation cost trajectories for adversarial perturbations are similar for ℓ_2 -optimized adversarial perturbations and ℓ_∞ -optimized adversarial perturbations.
5. Perturbation costs for random perturbations in ℓ_∞ norm decrease more slowly than those for ℓ_2 norm. For the model robustified to $\ell_\infty < 0.1$, the random perturbation cost trajectory mirrors that of the adversarial perturbations, but leads to misclassification in only approximately 10 % of cases.

By construction, adversarial examples are close to a decision boundary, but what about the rest of their surroundings? In Figure 6, we present perturbation cost trajectories for random perturbations *added to* adversarial perturbations. We observe that, although each adversarial example is misclassified (as that is how it was constructed), only a small fraction of points in its immediate vicinity are also misclassified. However, contrary to what we see for random perturbations added to the original inputs (cf. Figure 5), perturbation costs for random perturbations on top of adversarial perturbations do not decrease layer by layer – instead, the average perturbation cost trajectory for the adversarial perturbation with random noise follows the average perturbation cost trajectory for the adversarial perturbations. The two trajectories only separate in the argmax layer. This shows that perturbations in the general vicinity of the adversarial perturbation, are not abstracted away by the neural network processing, although most of them do not affect the final classification. We also observe that a much larger proportion of points in the vicinity of the adversarial examples for the ℓ_2 -robustified model are misclassified than for the ℓ_∞ -robustified model.

Since ℓ_∞ robustification also improves ℓ_2 robustness and vice versa (see Section 3), one might expect that adversarial examples themselves transfer between the models robustified for different norms. To explore this, we find adversarial perturbations for each trained model and calculate the respective trajectories not only for said model, but for *all three* models – see Figure 7. The adversarial perturbations are only successful against the models upon which they were created. In fact, both robustified models process “foreign” adversarial perturbations similarly to ℓ_∞ -scaled random perturbations. Perhaps surprisingly, the non-robust ST model manages to correctly classify almost all “foreign” adversarial examples, even though the perturbations are relatively large.

All in all, we observe that both models trained with MMR + AT have less variation in perturbation costs across layers than the non-robust ST model. We are surprised by how strongly the perturbation cost trajectory decreases for ℓ_2 -scaled random per-

³We limit our analysis to the least and most effective methods, respectively, because of computational (and time) constraints.

⁴See Appendices C.2 and C.3 for details on how we construct the perturbations.

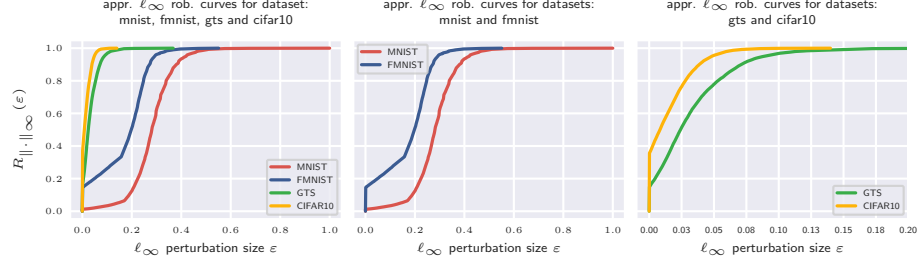


Figure 4: Approximated l_∞ robustness curves for multiple data sets. Each curve is calculated for a different model and a different test data set. The data sets are indicated by the labels. The models are trained with MMR + AT, Threat Models: MNIST: $\ell_\infty(\epsilon = 0.1)$, FMNIST: $\ell_\infty(\epsilon = 0.1)$, GTS: $\ell_\infty(\epsilon = 4/255)$, CIFAR-10: $\ell_\infty(\epsilon = 2/255)$.

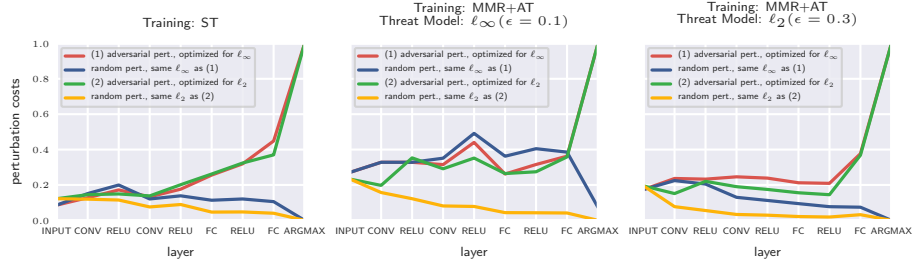


Figure 5: Averaged perturbation cost trajectories for adversarial and random perturbations for ST and AT. The labels of the curves show the perturbation type of the individual curves. The training methods are indicated by the subplot titles. In [Appendix D.3](#) we present an additional experiment to explore why the l_∞ -robustified model misclassifies a number of random l_∞ perturbations (middle).

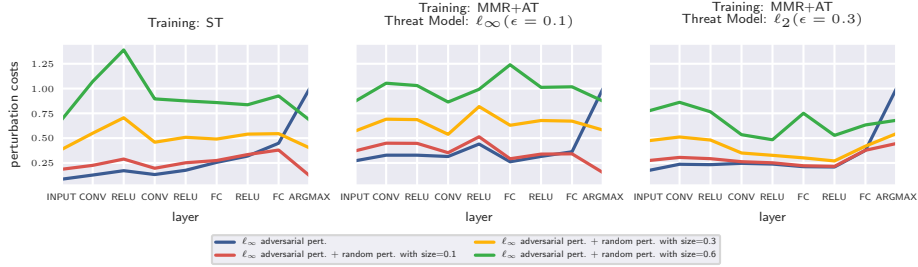


Figure 6: Perturbation cost trajectories for adversarial perturbations plus random perturbations of different sizes for different training methods. The labels of the curves show the perturbation type and random perturbation size of the individual curves. The training methods are indicated by the subplot titles.

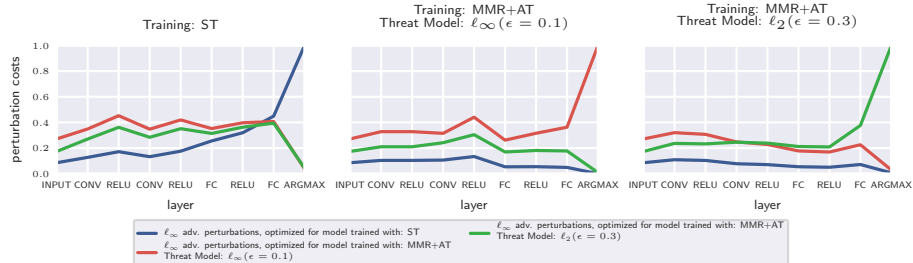


Figure 7: Perturbation cost trajectories for l_∞ adversarial perturbations (optimized for different threat models) for models trained with different training methods. The labels of the curves show the perturbation type and the model, for which the perturbation was optimized. The training methods are indicated by the column titles.

turbations, for all three models. Our finding that “foreign” adversarial examples are repelled is at odds with the observation that for black-box attacks, transfer of adversarial examples between different models seems to be crucial.

5 SCALE OF ROBUSTNESS CURVES

The dependence of scale on the norm

In [Section 3](#), we showed examples of how different the scale of robustness curves (as characterized, for example, by the average distance of a sample from a decision boundary) can be, both based on the distance function chosen as well as the data set under consideration. In the following, we present some considerations on how heavily scale may vary, and end with some practical recommendations for practitioners working with popular data sets. We begin by observing that on finite-dimensional vector spaces, one robustness curve places natural bounds on all others that represent distances induced by norms:

Proposition 1. *Let X be a finite-dimensional vector space. Let d and d' be two distance measures on X that are induced by norms. Then there exist constants $c_1, c_2 > 0$ such that for every classifier f ,*

$$R_{d'}^f(c_1\varepsilon) \leq R_d^f(\varepsilon) \leq R_{d'}^f(c_2\varepsilon) \quad \forall \varepsilon. \quad (3)$$

See [Appendix B.1](#) for the proof. Even restricting ourselves to ℓ_p norm-induced distances, it is clear that the bounds provided by [Proposition 1](#) are not necessarily informative. As noted in the discussion for [Theorem 1](#), even for this reduced class of distances, the constants c_1, c_2 can lead to a very broad range. For example, we find

$$R_{\|\cdot\|_\infty}^f(\varepsilon) \leq R_{\|\cdot\|_1}^f(\varepsilon) \leq R_{\|\cdot\|_\infty}^f(m\varepsilon) \quad (4)$$

where m is the data dimensionality, and these inequalities are tight. See [Appendix B.2](#) for an example of a data distribution where we construct two classifiers with identical ℓ_∞ robustness, but ℓ_1 robustness that differs by a factor of m . Consequently, at least in high dimensions, the scale of a robustness curve *can*, but *doesn't necessarily* depend strongly on the choice of norm.

Scale for specific data sets

Robustness curves allow us to analyze robustness globally, without focusing too much on (more or less) arbitrary thresholds. Nonetheless, the question of scale remains. Which perturbations should one consider “large” or “small”? One of the underlying assumptions in the definition of adversarial examples is that when $f(x') \neq y$, x' is being incorrectly classified, i. e. $f(x') = y$ would be the correct classification choice. The question of scale therefore cannot be answered independently of the data distribution. In order to understand how to interpret different perturbation sizes, it can be helpful to understand how strongly the data point would need to be perturbed to *actually* change the *correct* classification. In this section, we analyze this question for several popular data sets.

Recall that for two differently labeled points (x_1, y_1) and (x_2, y_2) , with $x_1 \neq x_2$ and $y_1 \neq y_2$, the perturbation $x_2 - x_1$ when applied to x_1 hopefully leads to a change in prediction, but it can hardly be considered adversarial. Instead, it can provide some sense

of scale and serve as an upper bound on reasonable robustness thresholds: when a perturbation is large enough to change an input such that the result should *correctly* be assigned a different label, it might not be sensible to expect a model to be robust against it. Similarly, when a perturbation does not even “reach” the closest point of the same label, it probably should not be able to influence a model’s prediction. Of course, this is subject to the concrete distribution in question and depends on the specific sampled data that is available.

When we look at the respective numbers for the MNIST test set in the ℓ_∞ , ℓ_2 , and ℓ_1 norms, we can make several observations. See [Figure 8](#) for the distributions of distances between points and their closest neighbors from the same class and different classes. Because the smallest inter-class distance in the ℓ_∞ norm is around 0.9, we can see that transforming an input from one class to one from a different class almost always requires completely flipping at least one pixel from almost-black to almost-white or vice versa. Transforming within a given class frequently requires only a smaller perturbation. For the ℓ_2 and ℓ_1 norms, the inter-class distance distributions are more spread out than the ℓ_∞ inter-class distance distribution. We observe that with ℓ_2 perturbations of size ≥ 3 , it becomes possible to transform samples from different classes into each other, so starting from this threshold, any classifier must necessarily trade off between accuracy and robustness.

Now that we have developed a certain sense of scale w. r. t. MNIST, let us compare it to two further data sets, namely GTS and TINY-IMG. We present the inter- and intra-class distance distributions in the ℓ_∞ norm (where all distances lie in the interval $[0, 1]$) in [Figure 9](#). The shapes of the curves differ strongly between data sets, and – most notably – for TINY-IMG, the distance of each point to the nearest neighbor from a different class is smaller than the distance to the nearest neighbor within the same class. Presumably, this is due to high data dimensionality, a large number of classes, and relatively large variation within a given class, when compared to MNIST – refer to [Table 1](#) for exact values.

Finally, we compare the inter-class distance distributions in ℓ_∞ , ℓ_2 , and ℓ_1 norm for all data sets considered in this work – see [Figure 10](#). We observe that for the ℓ_1 norm, the shape of the curves is similar across data sets, but their extent is determined by the dimensionality. In the ℓ_∞ norm, vastly different curves emerge for the different data sets. We hypothesize that, because the inter-class distance distributions vary more strongly for ℓ_∞ distances than for ℓ_1 distances, the results of robustifying a model w. r. t. ℓ_∞ distances may depend more strongly on the underlying data distribution than the results of robustifying w. r. t. ℓ_1 distances. This is an interesting avenue for future work. In any case, it is safe to say that, when judging the robustness of a model by a certain threshold, that number must be set with respect to the scale of the distribution the model operates on.

In [Table 1](#), we summarize the smallest and largest inter-class distances in different norms together with additional information about the size, number of classes, and dimensionality of the all the data sets we consider in this work. The values correspond directly to [Figure 10](#), but even in this simplified view, we can quickly make out key differences between the data sets. Compare, for example, MNIST and GTS: While it appears entirely reasonable to expect ℓ_∞ robustness of 0.5 for MNIST, the same

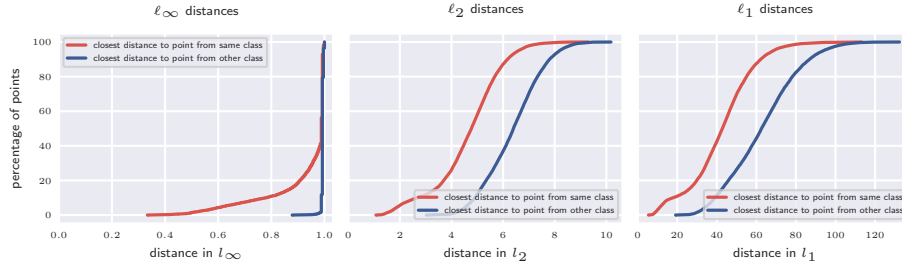


Figure 8: Minimum inter- and intra-class distances in different ℓ_p norms. Red curves: Sorted closest distances of each point to the closest point of the same class. Blue curves: Sorted closest distances of each point to the closest point of a different class. Left: Distance Measured in ℓ_∞ . Middle: Distance measured in ℓ_2 . Right: Distance measured in ℓ_1 . Data set is the full MNIST test set (10 000 points).

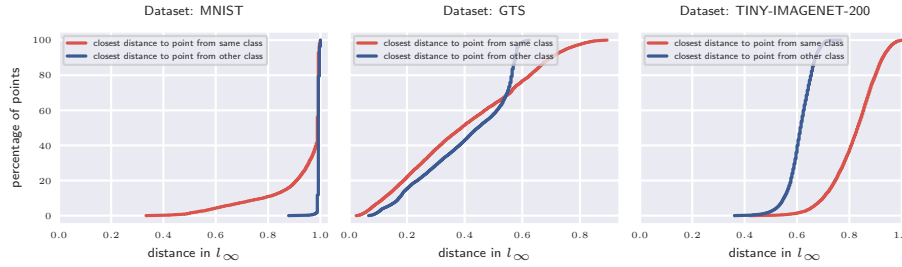


Figure 9: Minimum inter- and intra-class ℓ_∞ distances for three data sets. Red curves: Sorted closest ℓ_∞ distances of each point to the closest point of the same class. Blue curves: Sorted closest distances of each point to the closest point of a different class. Left: 10 000 points from MNIST test data set. Middle: 10 000 points from GTS test data set. Right: 9832 points from TINY-IMG test set.

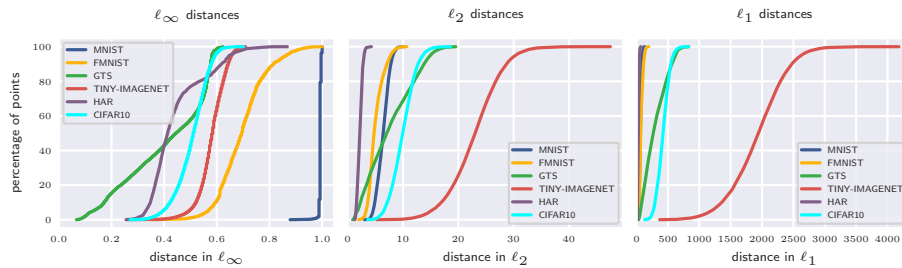


Figure 10: Minimum inter-class distances of all data sets considered in this work, measured in ℓ_∞ (left), ℓ_2 (middle), and ℓ_1 (right) norm. See Table 1 for size and dimensionality.

Table 1: Smallest and largest inter-class distances for subsets of several data sets, measured in l_∞ , l_2 , and l_1 norm, together with basic contextual information about the data sets. All data has been normalized to lie within the interval $[0, 1]$, and duplicates and corrupted data points have been removed. Besides HAR, all data sets contain images – the dimensionality reported specifies their sizes and number of channels.

Dataset	Samples	Classes	Dimensionality	l_∞	Inter-class Distance				
					Smallest		Largest		
					l_2	l_1	l_∞	l_2	l_1
MNIST	10 000	10	$28 \times 28 \times 1$	0.88	3.03	19.16	1.00	10.18	132.38
TINY-IMG	98 139	200	$64 \times 64 \times 3$	0.27	5.24	369.29	0.71	47.49	4184.37
FMNIST	10 000	10	$28 \times 28 \times 1$	0.36	2.00	24.87	1.00	10.70	194.29
GTS	10 000	43	$32 \times 32 \times 3$	0.07	0.90	31.46	0.62	19.54	833.22
CIFAR-10	10 000	10	$32 \times 32 \times 3$	0.27	3.61	130.77	0.70	18.57	831.44
HAR	2947	6	561	0.26	1.26	12.95	0.87	4.29	73.19

threshold for GTS is not possible. Relating Table 1 and Figure 4, we find entirely plausible the strong robustness results for MNIST, and the small perturbation threshold for GTS. Based on inter-class distances we also expect less l_∞ robustness for CIFAR-10 than for FMNIST, but not as seen in Figure 10.

Overall, the strong dependence of robustness curve scaling on the data set and the chosen norm, emphasizes the necessity of informed and conscious decisions regarding robustness thresholds. We hope that Table 1 can provide an easy reference when judging scales in a threat model.

6 CONCLUSION

We have investigated the relationships between adversarial defenses, the threat models they address, and the robustness of a model w. r. t. small perturbations in different norms, using robustness curves and perturbation cost trajectories. We have found that l_∞ threat models are surprisingly effective in improving robustness for other l_p norms, and hope that future defenses will be evaluated from this perspective. We have used perturbation cost trajectories to gain a broader view on how robust and non-robust networks perceive adversarial perturbations as opposed to random perturbations. Finally, we have seen how suitable robustness thresholds necessarily depend on the data set under consideration.

It is our hope that practitioners and researchers alike will use the methodology proposed in this work, especially when developing and analyzing adversarial defenses, and carefully motivate any threat models they might choose, taking into account the available context.

REFERENCES

- [1] Davide Anguita, Alessandro Ghio, Luca Oneto, Xavier Parra, and J Reyes-Ortiz. “A Public Domain Dataset for Human Activity Recognition using Smartphones”. In: *ESANN*. Jan. 2013.
- [2] Nicholas Carlini and David A. Wagner. “Towards Evaluating the Robustness of Neural Networks”. In: *2017 IEEE Symposium on Security and Privacy (SP)*. 2017. arXiv: [1608.04644](#).
- [3] Nicholas Carlini et al. *On Evaluating Adversarial Robustness*. 2019. arXiv: [1902.06705](#).
- [4] Pin-Yu Chen, Yash Sharma, Huan Zhang, Jinfeng Yi, and Cho-Jui Hsieh. *EAD: Elastic-Net Attacks to Deep Neural Networks via Adversarial Examples*. 2017. arXiv: [1709.04114](#).
- [5] Francesco Croce, Maksym Andriushchenko, and Matthias Hein. “Provable Robustness of ReLU networks via Maximization of Linear Regions”. In: *Proceedings of Machine Learning Research*. 2019. arXiv: [1810.07481](#).
- [6] Francesco Croce and Matthias Hein. “Provable robustness against all adversarial l_p -perturbations for $p \geq 1$ ”. In: *International Conference on Learning Representations*. 2020. arXiv: [1905.11213](#).
- [7] Elvis Dohmatob. “Generalized No Free Lunch Theorem for Adversarial Robustness”. In: *Proceedings of the 36th International Conference on Machine Learning*. 2019. arXiv: [1810.04065](#).
- [8] Ian J. Goodfellow, Jonathon Shlens, and Christian Szegedy. “Explaining and Harnessing Adversarial Examples”. In: *3rd International Conference on Learning Representations*. 2015. arXiv: [1412.6572](#).
- [9] Christina Göpfert, Jan Philip Göpfert, and Barbara Hammer. “Adversarial Robustness Curves”. In: *Machine Learning and Knowledge Discovery in Databases*. 2020. arXiv: [1908.00096](#).
- [10] Jan Philip Göpfert, André Artelt, Heiko Wersing, and Barbara Hammer. “Adversarial attacks hidden in plain sight”. In: *IDA*. 2020. arXiv: [1902.09286](#).
- [11] Pascale Gourdeau, Varun Kanade, Marta Kwiatkowska, and James Worrell. “On the hardness of robust classification”. In: *Advances in Neural Information Processing Systems*. 2019. arXiv: [1909.05822](#).
- [12] Sebastian Houben, Johannes Stallkamp, Jan Salmen, Marc Schlipsing, and Christian Igel. “Detection of Traffic Signs in Real-World Images: The German Traffic Sign Detection Benchmark”. In: *IJCNN*. 1288. 2013.
- [13] Diederik P. Kingma and Jimmy Ba. *Adam: A Method for Stochastic Optimization*. 2014. arXiv: [1412.6980](#).
- [14] Fei-Fei Li, Andrej Karpathy, and Justin Johnson. *CS231n: Convolutional Neural Networks for Visual Recognition*. [Online; accessed March 28, 2020]. 2016. URL: <http://cs231n.stanford.edu/2016/project.html>.
- [15] Aleksander Madry, Aleksandar Makelov, Ludwig Schmidt, Dimitris Tsipras, and Adrian Vladu. “Towards Deep Learning Models Resistant to Adversarial Attacks”. In: *ICLR*. 2018. arXiv: [1706.06083](#).

- [16] Jonas Rauber, Wieland Brendel, and Matthias Bethge. *Foolbox: A Python toolbox to benchmark the robustness of machine learning models*. 2017. arXiv: [1707.04131](#).
- [17] Christian Szegedy, Wojciech Zaremba, Ilya Sutskever, Joan Bruna, Dumitru Erhan, Ian J. Goodfellow, and Rob Fergus. *Intriguing properties of neural networks*. 2014. arXiv: [1312.6199](#).
- [18] Vincent Tjeng, Kai Y. Xiao, and Russ Tedrake. “Evaluating Robustness of Neural Networks with Mixed Integer Programming”. In: *International Conference on Learning Representations*. 2019. arXiv: [1711.07356](#).
- [19] Florian Tramer, Nicholas Carlini, Wieland Brendel, and Aleksander Madry. *On Adaptive Attacks to Adversarial Example Defenses*. 2020. arXiv: [2002.08347](#).
- [20] Eric Wong and Zico Kolter. “Provable Defenses against Adversarial Examples via the Convex Outer Adversarial Polytope”. In: *Proceedings of the 35th International Conference on Machine Learning*. 2018. arXiv: [1711.00851](#).

A PROOF OF THEOREM 1

Theorem 1. *If f is a linear classifier on \mathbb{R}^m parameterized by (\vec{w}, b) , i. e. $f(x) = \text{sgn}(\vec{w}^T x + b)$, then the shape of the robustness curve for f regarding an ℓ_p norm-induced distance does not depend on the choice of p . I.e. there exists a $c > 0$ such that*

$$R_{\|\cdot\|_{p_1}}^f(\varepsilon) = R_{\|\cdot\|_{p_2}}^f(c \cdot \varepsilon) \quad (5)$$

The distortion factor c is given by $\frac{\|w\|_{q_1}}{\|w\|_{q_2}}$, where $q_i = \frac{p_i}{p_i-1}$.

Lemma 1. *Let $x \in \mathbb{R}^m$ with $w^T x + b \neq 0$. Let $p \in [1, \infty]$ and q such that $\frac{1}{p} + \frac{1}{q} = 1$, where we take $\frac{1}{\infty} = 0$. Then*

$$\min\{\|\delta\|_p : \text{sgn}(w^T(x+\delta) + b) \neq \text{sgn}(w^T x + b)\} = \frac{|w^T x + b|}{\|w\|_q} \quad (6)$$

and the minimum is attained by

$$\delta = \begin{cases} \frac{-w^T x - b}{\|w\|_\infty} \text{sgn}(w_j) e_j, j = \arg\max_i |w_i| & p = 1 \\ \frac{-w^T x - b}{\|w\|_q^q} (\text{sgn}(w_i) |w_i|^{\frac{1}{p-1}})_{i=1}^d & p \in (1, \infty]. \end{cases} \quad (7)$$

where $x^{\frac{1}{\infty-1}} = x^0 = 1$ and e_j is the j -th unit vector.

Proof. By Hölder’s inequality, for any δ ,

$$\sum_{i=1}^m |w_i \delta_i| \leq \|\delta\|_p \|w\|_q. \quad (8)$$

For δ such that $\text{sgn}(w^T(x+\delta) + b) \neq \text{sgn}(w^T x + b)$ it follows that

$$\|\delta\|_p \geq \frac{\sum_{i=1}^m |w_i \delta_i|}{\|w\|_q} \geq \frac{|\sum_{i=1}^m w_i \delta_i|}{\|w\|_q} \geq \frac{|w^T x + b|}{\|w\|_q}. \quad (9)$$

Using the identity $q = \frac{p}{p-1}$, it is easy to check that for every $p \in [1, \infty]$, with δ as defined in Equation (7),

1. $w^T \delta = -w^T x - b$, so that $w^T(x+\delta) + b = 0$, and
2. $\|\delta\|_p = \frac{|w^T x + b|}{\|w\|_q}$.

Item 1 shows that δ is a feasible point, while Item 2 in combination with Equation (9) shows that $\|\delta\|_p$ is minimal. \square

Using Lemma 1, we are ready to prove Theorem 1.

Proof. By definition,

$$R_{\|\cdot\|_{p_1}}^f(\varepsilon) = P(\{(x, y) \text{ s.t. } \exists \delta : \|\delta\|_{p_1} \leq \varepsilon \wedge f(x+\delta) \neq y\}). \quad (10)$$

$\mathcal{R}_{p_1}(\varepsilon)$

We can split $\mathcal{R}_{p_1}(\varepsilon)$ into the disjoint sets

$$\underbrace{\{(x, y) : f(x) \neq y\}}_{=M} \quad (11)$$

$$\cup \quad (12)$$

$$\underbrace{\{(x, y) \text{ s.t. } \exists \delta : \|\delta\|_{p_1} \leq \varepsilon \wedge y = f(x) \neq f(x+\delta)\}}_{=B_{p_1}(\varepsilon)}. \quad (13)$$

Choose q_1, q_2 such that $\frac{1}{p_1} + \frac{1}{q_1} = 1$. By Lemma 1, and using that $f(x) = \text{sgn}(w^T x + b)$,

$$B_{p_1}(\varepsilon) = \{(x, y) : \text{sgn}(w^T x + b) = y \wedge \frac{|w^T x + b|}{\|w\|_{q_1}} \leq \varepsilon\} \quad (14)$$

$$= \{(x, y) : \text{sgn}(w^T x + b) = y \wedge \frac{|w^T x + b|}{\|w\|_{q_2}} \leq \frac{\|w\|_{q_1}}{\|w\|_{q_2}} \varepsilon\} \quad (15)$$

$$= B_{p_2}\left(\frac{\|w\|_{q_1}}{\|w\|_{q_2}} \varepsilon\right). \quad (16)$$

This shows that

$$R_{\|\cdot\|_{p_1}}^f(\varepsilon) = P(M) + P(B_{p_1}(\varepsilon)) \quad (17)$$

$$= P(M) + P\left(B_{p_2}\left(\frac{\|w\|_{q_1}}{\|w\|_{q_2}} \varepsilon\right)\right) \quad (18)$$

$$= R_{\|\cdot\|_{p_2}}^f\left(\frac{\|w\|_{q_1}}{\|w\|_{q_2}} \varepsilon\right). \quad (19)$$

\square

B ROBUSTNESS CURVE SEPARATION

B.1 Proof of Proposition 1

Proposition 1. *Let X be a finite-dimensional vector space. Let d and d' be two distance measures on X that are induced by norms. Then there exist constants $c_1, c_2 > 0$ such that for every classifier f ,*

$$R_{d'}^f(c_1 \varepsilon) \leq R_d^f(\varepsilon) \leq R_{d'}^f(c_2 \varepsilon) \quad \forall \varepsilon. \quad (20)$$

Proof. If X is a finite-dimensional vector space, it is known that any two norms on X are equivalent, i.e. for any two norms n, n' on X there exist constants $c_1, c_2 > 0$ such that for all $x \in X$

$$n(x) \leq c_1 n'(x) \text{ and } n'(x) \leq c_2 n(x). \quad (21)$$

For a distance function d and perturbation size ε , let

$$\mathcal{R}_d(\varepsilon) := \{(x, y) \text{ s.t. } \exists x' : f(x') \neq y \wedge d(x, x') \leq \varepsilon\}, \quad (22)$$

so that $R_d(\varepsilon) = P(\mathcal{R}_d(\varepsilon))$. Let d, d' be induced by the norms n, n' . If $(x, y) \in \mathcal{R}_{d'}(c_1 \varepsilon)$, it follows that $(x, y) \in \mathcal{R}_d(\varepsilon)$, and if $(x, y) \in \mathcal{R}_d(\varepsilon)$, it follows that $(x, y) \in \mathcal{R}_{d'}(c_2 \varepsilon)$. As a result,

$$R_{d'}^f(c_1 \varepsilon) \leq R_d^f(\varepsilon) \leq R_{d'}^f(c_2 \varepsilon). \quad (23)$$

\square

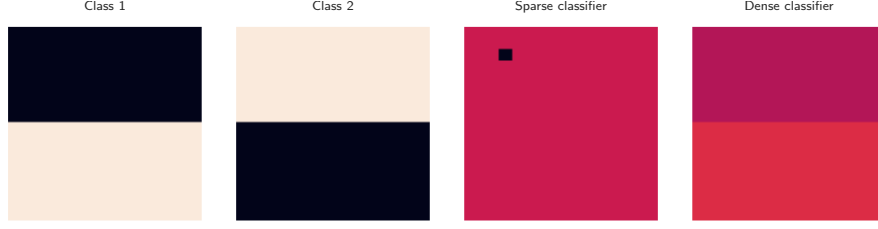


Figure 11: Left two images: the types of images distinguished between in the toy classification problem. Second from the right: a sparse weight vector, the result of a ℓ_1 -regularized linear SVM, with one non-zero entry. Right: a dense weight vector, the result of a ℓ_2 -regularized linear SVM, with no non-zero entries. The vectors are reshaped to 16×16 . Black corresponds to -1 , beige corresponds to 1 , and reddish colors correspond to values 0 or close to 0 .



Figure 12: Left: an image that is incorrectly classified by the sparse classifier, but not the dense classifier. Right: an image that is misclassified by both classifiers.

B.2 Example of robustness curve separation

As an illustrative toy example of how strongly the robustness curves for different norms can be separated, consider the following classification task. The goal is to distinguish between the two types of 16×16 -pixel images in Figure 11. Running a ℓ_1 -regularized linear SVM on this data leads to the sparse weight vector schematically represented in Figure 11, with just one non-zero entry. Running a ℓ_2 -regularized linear SVM leads to the dense weight vector also schematically represented in Figure 11, with all non-zero entries.

Both classifiers have 100% accuracy, and all samples are at ℓ_∞ -distance 1 from both decision boundaries, i.e. the ℓ_∞ robustness curves of both classifiers are identical. However, the ℓ_1 robustness curves of the two classifiers are maximally separated: for the sparse classifier, the ℓ_1 robustness curve is a step function at 1, while for the dense classifier, it is a step function at 256, the dimensionality of the data. Figure 12 shows adversarial examples for the two classifiers. For the sparse classifier, it is sufficient to flip a single pixel, while for the dense classifier, more noticeable changes are necessary.

C EXPERIMENTAL DETAILS

C.1 Model training

We use the same model architecture as [5] and [20]. Unless explicitly stated otherwise, the trained models are taken from [5]. The exact architecture of the model is: Convolutional layer (number of filters: 16, size: 4×4 , stride: 2), ReLu activation

function, convolutional layer (number of filters: 32, size: 4×4 , stride: 2), ReLu activation function, fully connected layer (number of units: 100), ReLu activation function, output layer (number of units depends on the number of classes). All models are trained with Adam Optimizer [13] for 100 epochs, with batch size 128 and a default learning rate of 0.001. More information on the training can be found in the experimental details section of the appendix of [5]. All models are publicly available in the GitHub repositories of [5] and [6]: www.github.com/max-andr/provable-robustness-max-linear-regions and www.github.com/fra31/mmr-universal.

C.2 Approximated robustness curves

We use state-of-the-art adversarial attacks to approximate the true minimal distances of input datapoints to the decision boundary of a classifier for our adversarial robustness curves (see Definition 1). We base our selection of attacks on the recommendations of [3]. Specifically, we use the following attacks: For ℓ_1 robustness curves we use EAD, [4], for ℓ_2 robustness curves we use [2] and for ℓ_∞ robustness curves we use [15]. For all three attacks, we use the implementations of Foolbox [16]. For the ℓ_∞ attack, we use the standard hyperparameters of the Foolbox implementation. For the ℓ_1 and ℓ_2 attacks we increase the number of binary search steps that are used to find the optimal tradeoff-constant between distance and confidence from 5 to 10, which we found empirically to improve the results. For the rest of the hyperparameters, we again use the standard values of the Foolbox implementation.

C.3 Generating random perturbations

We compare perturbation cost trajectories for adversarial perturbations and random perturbations. In the following, we specify how the random perturbations are generated. Let Δ be the perturbation that we want to generate. Δ is a m -dimensional vector, where m is defined by the number of input features of the original input. Let s be the target size of the noise.

If the target size is measured in ℓ_∞ norm, we sample

$$\Delta \sim s \cdot (\sigma_i)_{i=1}^m \quad (24)$$

where the σ_i are i.i.d. Rademacher variables, i.e. uniformly distributed on $\{\pm 1\}$. This method of sampling is based on the Fast Gradient Sign Method, and means that our random noise is large as possible under the ℓ_∞ norm constraints we impose.

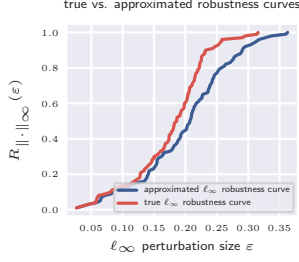


Figure 13: True and approximated robustness curves for ℓ_∞ norm. The model is trained on MNIST with MMR+AT, Threat Model: $\ell_\infty(\epsilon = 0.1)$. We use a different model architecture to reduce the runtime of the exact robustness evaluation. The model architecture is: INPUT, FC(1024), RELU. Both curves are calculated for 100 points of the MNIST test set. The true robustness curve is calculated using the Mixed Integer Programming method from [18]. The approximated curve is calculated using the PGD attack described in [15].

If the target size is measured in ℓ_2 norm, we let

$$\Delta = s \cdot \frac{X}{\|X\|_2} \quad (25)$$

where $X \sim \mathcal{N}_m(0, I_m)$, i. e. we sample a vector from a Gaussian distribution and scale it to the desired length.

C.4 Computational architecture

We executed all programs on an architecture with 2 x Intel Xeon(R) CPU E5-2640 v4 @ 2.4 GHz, 2 x Nvidia GeForce GTX 1080 TI 12G and 128 GB RAM.

D ADDITIONAL EXPERIMENTS

D.1 Justifying approximated robustness curves

We’ve compared approximated and true ℓ_∞ curves to justify our use of approximate robustness curves. For computational reasons, this was done only for MNIST, and for a smaller architecture than our other experiments, and not for ℓ_2 curves. The results can be seen in Figure 13. We observe that the curves track each other reasonably well, especially for small perturbation sizes, which is the most interesting region. Due to computational constraints, we did not perform this comparison for the more complicated architecture our other experiments are based on. The calculation of the exact robustness curve in Figure 13 took 2 days and 22 hours on our computational setup (see Appendix C for details). We started calculation of the exact curves for the architecture used in our other experiments, but had to cancel after 14 days, since not even a single data point had been evaluated.

D.2 Adversarial attack intuition

In order to provide intuition on how adversarial examples differ based on the choice of norm and defense, we show adversarial attacks to an image from GTS in Figure 14.

D.3 Distinguishing between defended and non-defended adversarial perturbations

Figure 5 gives the impression that the MMR + AT (ℓ_∞) model does not reduce perturbation costs of random ℓ_∞ perturbations as the other models do (although only a small number of these perturbations lead to misclassification). To verify that this is not simply due to the larger perturbation size made necessary for the robustified model, we calculate perturbation cost trajectories separated by the size of the adversarial perturbation (defended against or part of the percentage not defended against). For both cases, and thus for both perturbation magnitudes, we observe the same effect.

D.4 Calculating inter-class distances

In Figure 16, we show minimum inter-class distances of ℓ_∞ , ℓ_2 and ℓ_1 norm for subsets of commonly used data sets. We can observe, that for all norms and all data sets we examined, a small sample (10 % to 25 %) of the data is sufficient to reliably estimate the minimum inter-class distance of the full data set.

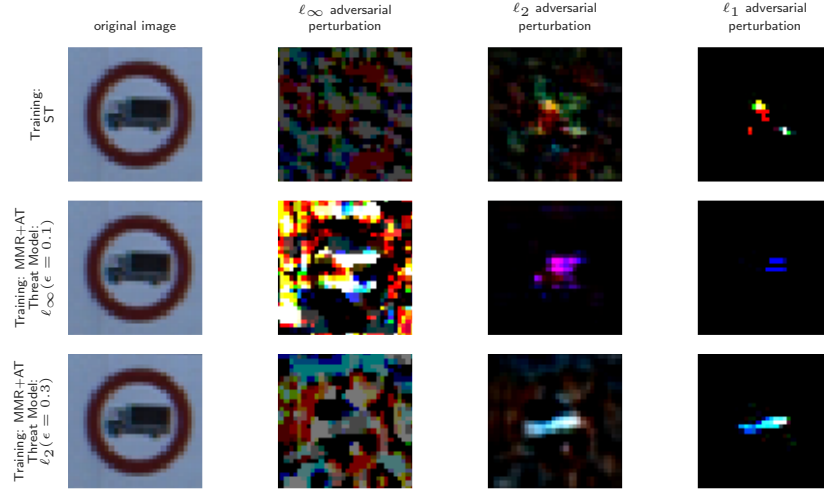


Figure 14: Adversarial examples for robust/non-robust models and different norms. The adversarial examples are generated with adversarial attacks (ℓ_∞ : Projected Gradient Descent Attack (PGD) as suggested in [15], ℓ_2 : Carlini Wagner L2 Attack (CW) as suggested in [2], ℓ_1 : Elastic-net attack (EAD) as suggested in [4]). The adversarial perturbations are scaled by factor 10 to increase visibility. We show adversarial examples for three different models. The training methods are indicated by the labels on the y-axes. The original image is taken from GTS.

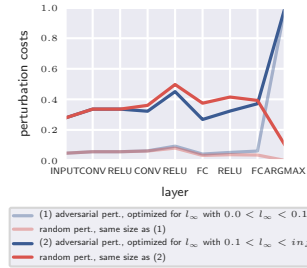


Figure 15: Perturbation cost trajectories for ℓ_∞ adversarial perturbations and random perturbations for a robust model, separated by class (defended against vs. not defended against). The curves show the mean perturbation costs for a subset of 1000 datapoints of the MNIST test set, that falls into the respective class. The labels of the curves show the perturbation type and the class of the individual curves. The model is trained with MMR+AT, Threat Model: $\ell_\infty(\epsilon = 0.1)$.

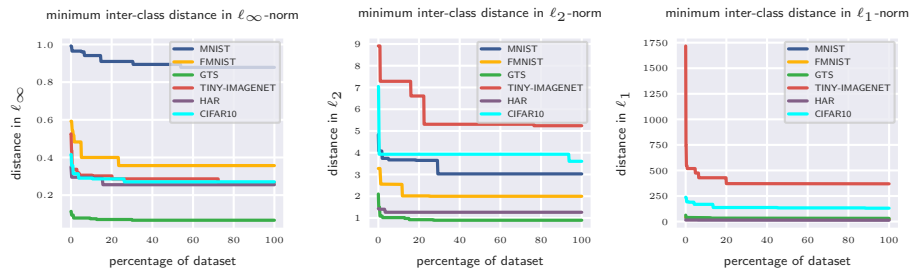


Figure 16: Minimum inter-class differences for subsets of different data sets, measured in ℓ_∞ , ℓ_2 and ℓ_1 norm.